Modeled variations of the inherent optical properties of summer Arctic ice and their effects on the radiation budget: A case based on ice cores from CHINARE 2008–2016

Miao Yu[1], Peng Lu[1]*, Matti Leppäranta[2], Bin Cheng[3], Ruibo Lei[4], Bingrui Li[4], Qingkai Wang[1], Zhijun Li[1]*

[1]State Key Laboratory of Coastal and Offshore Engineering, Dalian University of Technology, Dalian, China
[2]Institute of Atmosphere and Earth Sciences, University of Helsinki, Helsinki, Finland
[3]Finnish Meteorological Institute, Helsinki, Finland
[4]MNR Key Laboratory for Polar Science, Polar Research Institute of China, Shanghai, China

Corresponding to: Peng Lu (lupeng@dlut.edu.cn), Zhijun Li (lizhijun@dlut.edu.cn).

Abstract. Variations in Arctic sea ice are not only apparent in its extent and thickness but also in its internal properties under global warming. The microstructure of summer Arctic sea ice changes due to varying external forcing, ice age, and extended melting seasons, which affect its optical properties. Sea ice cores sampled in the Pacific sector of the Arctic obtained by the Chinese National Arctic Research Expeditions (CHINARE) during the summers of 2008 to 2016 were used to estimate the variations in the microstructures and inherent optical properties (IOPs) of ice and determine the radiation budget of sea ice based on a radiative transfer model. The variations in V_a of the ice top layer were not significant and V_a of the ice interior layer was significant. Compared with 2008, the mean V_a of interior ice in 2016 decreased by 9.1%. Meanwhile, the volume fraction of brine pockets increased clearly in the study years. The changing microstructure resulted in the scattering coefficient of the interior ice decreasing by 38.4% from 2008 to 2016, while no clear variations can be seen in the scattering coefficient of the ice top layer. These estimated ice IOPs fell within the range of other observations. Furthermore, we found that variations in interior ice were significantly related to the interannual changes in ice ages. At the Arctic basin scale, the changing IOPs of interior ice greatly changed the amount of solar radiation transmitted to the upper ocean even when a constant ice thickness is assumed, especially the thin ice in marginal zones, implying the presence of different sea ice bottom melt processes. These findings revealed the important role of the changing microstructure and IOPs of ice in affecting the radiation transfer of Arctic sea ice.

1 Introduction

The recent rise in air temperature in the Arctic is almost twice the global average, known as Arctic amplification (Dai et al., 2019), which has been seen in the retreat of sea ice, especially in summer. The extent of sea ice in summer has decreased (Comiso et al., 2008; Parkinson & Comiso, 2013; Petty et al., 2018), and summer ice is thinner (Kwok, 2018), younger (Stroeve and Notz, 2018), and warmer (Wang et al., 2020) than before. These changes have affected the transfer of sunlight into the Arctic Ocean, and the optical properties of sea ice are changing the solar radiation budget in the area.

Variations of Arctic sea ice cover are related not only to the macroscale properties described above but also to the ice microstructure. Sea ice is a multiphase medium consisting of pure ice, gas bubbles, brine pockets, salt crystals, and sediments (Hunke et al., 2011). In the last decades, the length of the Arctic ice melt season has shown a significant positive trend (Markus et al., 2009), and the Arctic ice cover has experienced a transition from predominantly old ice to primarily first-year ice (Stroeve and Notz, 2018; Tschudi et al., 2020). At the same time, in melting ice gas bubbles and brine pockets tend to become larger (Light et al., 2003), and phase changes due to brine drainage and temperature result in variations in the volume of gas and brine (Weeks and Ackley, 1986; Crabeck et al., 2019). Except for the above-mentioned factors, absorption of shortwave radiation, synoptic weather, and surface melt pooling can also partly affects the ice microstructure. Therefore, the physical properties of ice have changed and in the past 10 years the bulk density of summer Arctic sea ice has been lower than reported in the 1990s due to increased ice porosity (Wang et al., 2020). Despite the changing ice microstructure having attracted attention, there is still no quantitative description of its evolution and effect factors (Petrich and Eicken, 2010).

Gas bubbles and brine pockets, as dominant optical scatterers, directly influence the inherent optical properties (IOPs) of sea ice (Grenfell, 1991; Perovich, 2003). IOPs include scattering and absorption coefficients and information about the phase function of the domain. The varying IOPs of ice have attracted attention due to their important role in the process of light penetration in ice. Light et al. (2008) and Katlein et al. (2019; 2021) demonstrated clear different IOPs in sea ice of different depth. The differences in the IOPs between first-year ice and multiyear ice have been ascertained in many observations (e.g., Light et al., 2015; Grenfell et al., 2006). There are also some differences in the bulk IOPs of first-year ice because of the different stages of melting (Veyssière et al., 2022). Whereas, the available observed or estimated ice IOPs were rare, which results in quantitative knowledge of the progression of the sea ice IOPs and their influencing factors was still absent (light et al. 2015). Even in the latest studies and sea ice models, IOPs are set as constants based on previous field observations (e.g., Briegleb & Light, 2007), which is somewhat in contrast to the reality in the Arctic Ocean.

Changes in ice microstructure or IOPs are especially important for the energy budget of Arctic ice under the general warming climate and decreasing ice age. The reason for this is their direct effect on ice apparent optical properties (AOPs), which influence the partitioning of radiation in the Arctic by various feedback processes. Whereas, the observed relationships between ice microstructure, IOPs, and AOPs are rare in the available literature. Parameterization proposed by Grenfell (1991) was the most widely used method to estimate the response of ice IOPs to microstructure. Due to the lack of detailed, observed ice microstructure, this method was usually used to build models (e.g. Hamre, 2004; Light et al., 2004; Yu et al., 2022). In the latest MOSAiC expedition during 2019-2020, Smith et al. (2022) observed the formation of a porous surface layer (i.e. surface scattering layer, SSL) of sea ice and its enhancement on ice albedo. Macfarlane et al. (2023) further detailly described the microstructure of SSL using X-ray tomography and its effects on ice optical properties. They are the first to link ice microstructure and optical properties by field observations.

In this study, *in situ* observations of the physical properties of summer Arctic sea ice during the Chinese National Arctic Research Expeditions (CHINARE) from 2008 to 2016 were employed as input data. Variations of the microstructure and the IOPs of Arctic sea ice are presented. Also shown are their quantitative effects on the radiation budget in the area. Applying these varying IOPs to satellite-observed sea ice conditions has allowed us to obtain Arctic-wide estimates of the role of ice microstructure in the radiation budget of the region.

2 Data and method

2.1 Arctic sea ice coring

The Arctic sea ice cores were sampled in the Pacific sector of the Arctic Ocean during summer cruises of the CHINARE program from 2008 to 2016 (Figure 1). Detailed volume fractions of the gas bubbles and brine pockets (V_a, V_b) in the ice cores were given by Wang et al. (2020). The mean sampling date of ice cores was Aug. 20 ± 8 days, when the ice had been melting for a while (~59 days) and had not yet begun to freeze according to the melting onset data from NASA. According to previous observations, there are no clear temporal changes in the microstructure of surface ice in the entire July (Macfarlane et al., 2023). Furthermore, the ice surface melt rate in August was only ~1/10 of that in July (Perovich, 2003; Nicolaus et al., 2021). Therefore, short-term temporal variability was expected not to affect surface ice microstructure obviously.

To further reduce the impact of temporal variations in the ice cores on the ice microstructure, we preprocessed the ice core data. The ice cores in each year were allocated different weights according to their sampling date. The weight (w) of ice cores in affecting period (D) can be got according to the Cressman method: $w = \frac{D^2 - d^2}{D^2 + d^2}$, where d is the number of days from the mean sampling date. The D was set to 30 days empirically. Then the weighted mean of ice properties was $\bar{x} = \frac{\sum_{i=1}^{n} w_i x_i}{\sum_{i=1}^{n} w_i}$. In the following analyses, the mean values of each year refer to the weighted ones. After the preprocessing, the deviation of melting days in a single year was reduced by ~50.5%. As for the spatial variations in the ice cores, it is difficult for field observations to avoid the effects of spatial variations. Therefore, related studies have generally ignored the effects of sampling locations on the statistics (e.g. Carnat et al., 2013; Frantz et al., 2019; Katlein et al., 2019; Light et al., 2022). Related discussion about the temporal and spatial variations can be found in Section 4.2.

A typical undeformed sea ice floe consists texturally of three layers due to its growth conditions (Tucker et al., 1992). The first two layers are relatively thin and consist of a granular layer and a transition layer, and the lowest layer generally consists of columnar ice. The ice texture controls the ice microstructure (Crabeck et al., 2016). Thus, the development of gas bubbles, brine pockets, and IOPs in the three ice layers is different. Analogous to the parameterization of the Los Alamos sea ice model (CICE; Briegleb & Light, 2007), Each ice core was evenly divided into 10 layers. The top (1/10) layer of an ice core was defined as the top layer (TL), the second layer (2/10) was the drained layer (DL), and layers 4–10/10 collectively constitute the internal layer (IL). Note that the surface scattering layer (SSL) and part of the DL were mixed in the TL and could not be separated completely. Layer 3/10 was also a mixture of a DL and IL, and is therefore neglected in the following analysis.

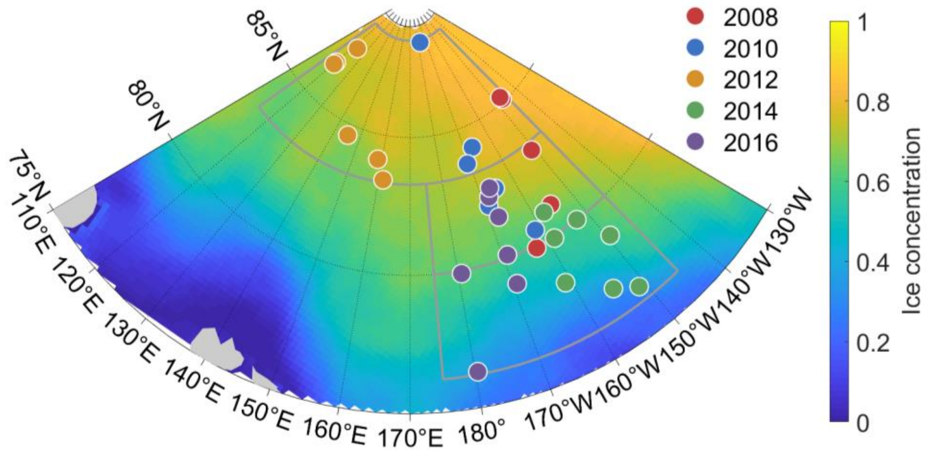

Figure 1. Locations of the sampled ice cores during CHINARE cruises. The ice cores were assorted into three parts according to latitude and ice concentration. Their quantities were nearly the same in each zone. The ice concentration in the base map was the mean in August from 2008 to 2016.

2.2 Sea ice optics modeling

The IOPs of sea ice, including the scattering coefficient, σ, absorption coefficient, κ, and asymmetry parameter, g, can be determined directly from the ice microstructure. Following the theory of Grenfell (1991), scattering in ice is caused by gas bubbles and brine pockets, and absorption is caused by brine pockets and pure ice. This parameterization has been proved by extensive observations (e.g., Light et al., 2004; Smedley et al., 2020). The IOPs of sea ice can be obtained from the sum of the scatterers weighted by their relative volumes as:

$$\sigma = \sigma_\mathrm{a} + \sigma_\mathrm{b} = \int_{r_\mathrm{min}}^{r_\mathrm{max}} \pi r_\mathrm{a}^2 Q_\mathrm{a}^\mathrm{sca} N_\mathrm{a}(r) dr + \int_{l_\mathrm{min}}^{l_\mathrm{max}} \pi r_\mathrm{b}^2 Q_\mathrm{b}^\mathrm{sca} N_\mathrm{b}(l) dl \tag{1}$$

$$\kappa = \kappa_\mathrm{i} + \kappa_\mathrm{b} = k_\mathrm{i} V_i + \int_{l_\mathrm{min}}^{l_\mathrm{max}} \pi r_\mathrm{b}^2 Q_\mathrm{b}^\mathrm{abs} N_\mathrm{b}(l) dl \tag{2}$$

$$g = \frac{g_\mathrm{a}\sigma_\mathrm{a} + g_\mathrm{b}\sigma_\mathrm{b}}{\sigma} \tag{3}$$

In these equations, the subscripts a and b represent gas bubbles and brine pockets, respectively, r is their radius (or equivalent radius), and l is the length of the brine pockets. Q^{sca} and Q^{abs} are the scattering and absorption efficiencies, respectively, which can be calculated using Mie theory. N is the size distribution function, subscript i represents pure ice, and $V_i = 1 - V_a - V_b$ is its volume fraction. The values of these parameters are summarized in Table 1. Brine pockets longer than 0.03 mm are modeled as cylinders rather than spheres (Light et al. 2003). The conversion function from Grenfell & Warren (1999) is employed to represent hexagon columns as spheres with the same optical properties. Besides, Q^{abs} and Q^{sca} in the required size range are obtained using their effective radii, which are calculated according to Hansen & Travis (1974).

Table 1. Parameters used in the radiation transfer model in Arctic summer and their sources

Parameter	Reference(s)
refractive index of gas bubbles	Light et al. (2004)
refractive index of brine pocket	Smith and Baker (1981)
N_a, N_b	Light et al. (2003)
k_i	Grenfell and Perovich (1981)
g_a, g_b	Light et al. (2004)
r_{min} = 0.5 mm, r_{max} = 2 mm	Grenfell (1983); Frantz et al. (2019)
l_{min} = 1 mm, l_{max} = 20 mm	Light et al. (2003); Frantz et al. (2019)

The Delta-Eddington multiple scattering model, where the constant IOPs from Briegleb & Light (2007) were replaced by the modeled IOPs, was employed to estimate the apparent optical properties (AOPs: albedo α_λ, transmittance T_λ, and absorptivity A_λ) of the ice at the sampling sites (Yu et al., 2022). This radiative transfer model was commonly used, and its accuracies were widely accepted. The integrated albedo (α_B), transmittance (T_B), and absorptivity (A_B) were calculated by integrating the spectral values over the band of the incident solar radiation, F_0 as:

$$X_B = \frac{\int_{\lambda_1}^{\lambda_2} X_\lambda F_0(\lambda) d\lambda}{\int_{\lambda_1}^{\lambda_2} F_0(\lambda) d\lambda}, X = \alpha, T, A, \tag{4}$$

In the following sections, the integrated absorption coefficient, κ_B, was also derived by this equation, following CICE (Briegleb & Light, 2007). Considering the generally cloudy weather in Arctic summer, the incident solar irradiance under an overcast sky in August from Grenfell & Perovich (2008) was chosen as the default value for F_0. The studied wavelength band was set as the photosynthetically active band, i.e. λ_1 = 400 nm and λ_2 = 700 nm.

2.3 Arctic-wide up-scaling

To conduct an up-scaling analysis of the radiative budget of the Arctic sea ice cover based on observations of the ice microstructure in the Pacific sector, we used representative basin-scale sea ice data to estimate the variations in the distribution of radiation fluxes in summer during 2008-2016. The sea ice concentration (C) was provided by the National Snow and Ice Data Center (NSIDC) (DiGirolamo et al., 2022), the sea ice thickness was based on CryoSat-2/SMOS data fusion (Ricker et al., 2017), and the downward shortwave radiation flux at the surface (E_d) was obtained from the European Centre for Medium-Range Weather Forecasts (ECMWF). The latter two datasets were interpolated to a 25 km NSIDC Polar Stereographic grid. Then, the mean radiation fluxes and ice concentrations from July to September from 2008 to 2016 were set as the representative values in summer. Due to the limitation of satellite remote-sensing data of summer ice thickness, the representative thickness was estimated according to the mean value in October from 2011 to 2016, together with the growth rate estimated by Kwok and Cunningham (2016). Then, representative ice thickness can be got. These grided ice thickness and IOPs profiles from ice cores were inputted in the radiative transfer model to estimate the ice AOPs. From all these data sets and the derived parameters, the reflected, absorbed, and transmitted radiation flux by Arctic sea ice were calculated as $E_r = E_d \cdot C \cdot \alpha_B$, $E_a = E_d \cdot C \cdot A_B$, and $E_t = E_d \cdot C \cdot T_B$, respectively.

3 Results

3.1 Microstructure of the ice cores

There were different variation trends in the volume fraction of gas bubbles and brine pockets (V_a, V_b) as a function of ice core depth (Figure 2). The upper granular ice was typically bubbly, associated with the drainage of brines, and the interior columnar ice is usually depleted in gas bubbles (Cole et al., 2004). Thus, a significantly different V_a could be seen (Analysis of variance (ANOVA), $P < 0.01$) with a decreasing trend along depth (Pearson correlation coefficient, $r = -0.97$, $P < 0.01$). The mean V_a of the TL, DL, and IL for all ice cores was 23.4 ± 5.6%, 17.9 ± 5.3%, and 11.6 ± 5.9%, respectively. These values are similar to the observations made by Eicken et al. (1995) where V_a decreased from > 20 % at the top to < 5 % at the bottom for summer Arctic sea ice.

The different V_b between layers was significant (ANOVA, $P < 0.01$). The drainage of brine resulted in a relatively small V_b of TL, with a mean of 3.5 ± 2.4%, while it was 4.6 ± 3.1% and 13.5 ± 6.7% in the other two layers, respectively (Figure 2a). V_b = 5% is usually chosen as a threshold where discrete brine inclusions start to connect and the columnar ice is permeable enough to enable drainage (Carnat et al., 2013). Thus, the ice cores in the present study have been melting for some time, agreeing with the sampling season during CHINARE. Most V_b profiles had a maximum in the middle depth, except for the ice cores in 2012 (Figure 2d). This can be explained by the later sampling date in 2012 relative to the other years by about 10 days, which resulted in enhanced brine drainage. Furthermore, the shape of the V_b profile was also associated with the ice age (Notz and Worster, 2009). Compared with the ice cores in 2010, although the ice cores in 2016 had similar sampling dates (one day difference), the maximum position of V_b in 2016 was lower than in 2010 (Figure 2c, f). This was because all ice cores in 2010 were sampled from first-year ice, and the ice cores in 2016 were comprised of first-year ice and multiyear ice (Wang et al., 2020).

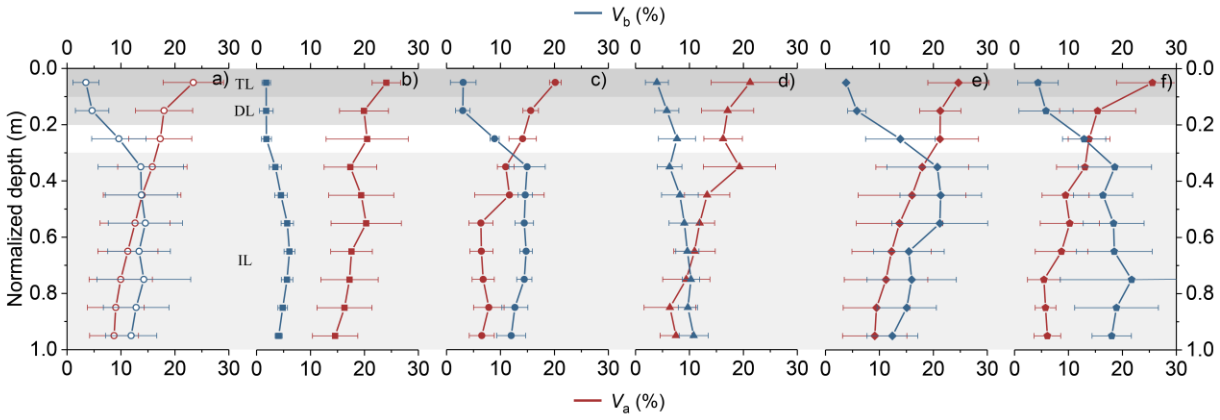

Figure 2. Profiles of V_a and V_b against normalized depth in (a) the whole study period, (b) 2008, (c) 2010, (d) 2012, (e) 2014, and (f) 2016. The error bars show the standard deviation from the mean of the results. The shady areas represent the ice layer structure.

In addition to the different variations in V_a and V_b with depth, the annual variations in each layer were also different (Figure 3a). V_a was relatively small in the TL of 2010 because all ice cores were sampled from first-year ice (Wang et al., 2020). The quantities of first-year ice cores were similar to the amount of multiyear ice cores in the other years. The variation in V_a of TL between years was statistically insignificant (ANOVA, $P > 0.1$). This indicated that the melting process of the ice surfaces of the cores in different years was not different significantly. Contrary to the TL, the V_a in the IL was different significantly (ANOVA, $P < 0.05$). Compared with 2008, the mean V_a of IL in 2016 decreased by 9.1%. The V_a values of DL were relatively stable and did not show significant variations in the study period.

Things were different for V_b and ice porosity. There were increases in the mean V_b of all three ice layers (Figure 3b). Furthermore, the increases of mean V_b in the IL were statistically significant ($r = 0.84$, $P < 0.1$; ANOVA, $P < 0.01$). From 2008 to 2016, the increase in the mean V_b of IL was 13%. Simultaneously, the ice salinity of the IL decreased (Figure S1), which agreed well with the observed and modeled results with warming conditions (e.g., Vancoppenolle et al., 2009). From the combined effects of changing V_a and V_b, there are no significant differences in the porosity of three layers (ANOVA, $P >$ 0.1). Furthermore, the developments of porosity in the three layers are also similar (Figure 3c). Among the three layers, the statistical significance of changing porosity of IL between years was relatively well (ANOVA, $P < 0.1$).

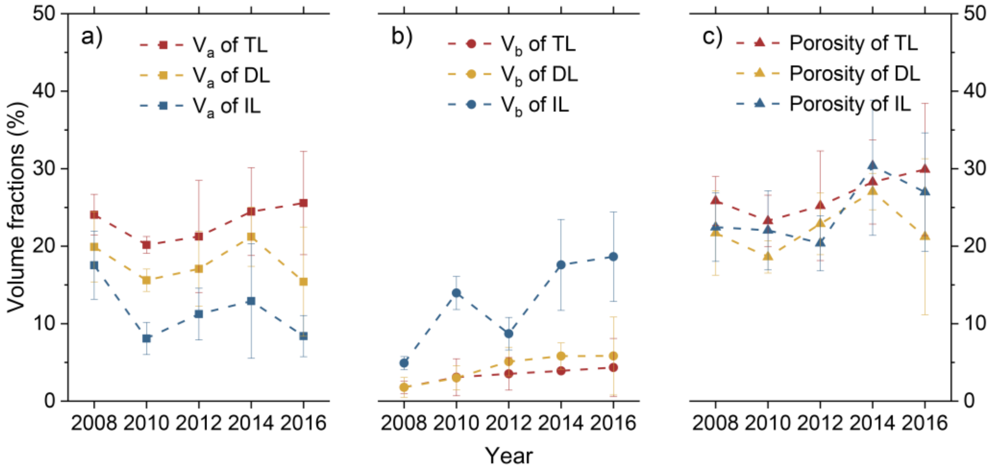

Figure 3. Variations in (a) V_a, (b) V_b, and (c) the porosity of the TL, DL, and IL of the ice cores during 2008-2016. The error bars show the standard deviation for each year.

3.2 Variations in the IOPs of the ice cores

The mean scattering coefficient, σ, of the TL, DL, and IL for all ice cores was 264.5 ± 26.7 m^{-1}, 208.9 ± 26.5 m^{-1}, and 160.9 ± 33.3 m^{-1}, respectively (Figure 4a). There was a significant decreasing tendency along with depth in the mean σ of all ice cores (r = -0.97, $P < 0.01$; ANOVA, $P < 0.01$), associated with a decreasing volume of gas bubbles (Figure 2). Although the V_b values of the ice cores increased clearly with depth, their effects on ice σ were covered by the decreasing V_a. The reason for this was that the refractive indices of brine pockets and pure ice are close (Smith and Baker, 1981; Grenfell and Perovich, 1981), which results in the effects of brine pockets on ice σ were relatively weak than the gas bubble.

The vertical variations in κ_B and g were not clear as seen for σ because they depend on V_i and V_b/V_a, respectively. Due to the effects of the ice porosity ($V_a + V_b$), κ_B didn't show a statistically significant trend with depth (ANOVA, $P > 0.1$), which varied in the range 0.09–0.1 m^{-1}. The mean value of g was 0.93 except in 2008 (which was g = 0.89), and it significantly increase with depth (r = 0.91, $P < 0.01$; ANOVA, $P < 0.01$). This value is similar to the commonly used one; for example, the previous typical range of g was from 0.86 to 0.99 (e.g., Ehn et al., 2008), and 0.94 was often adopted for computational efficiency in models (Light et al., 2008). We note that the volume of brine pockets in ice cores of 2008 is relatively small, which was a reason for the different values of g found here.

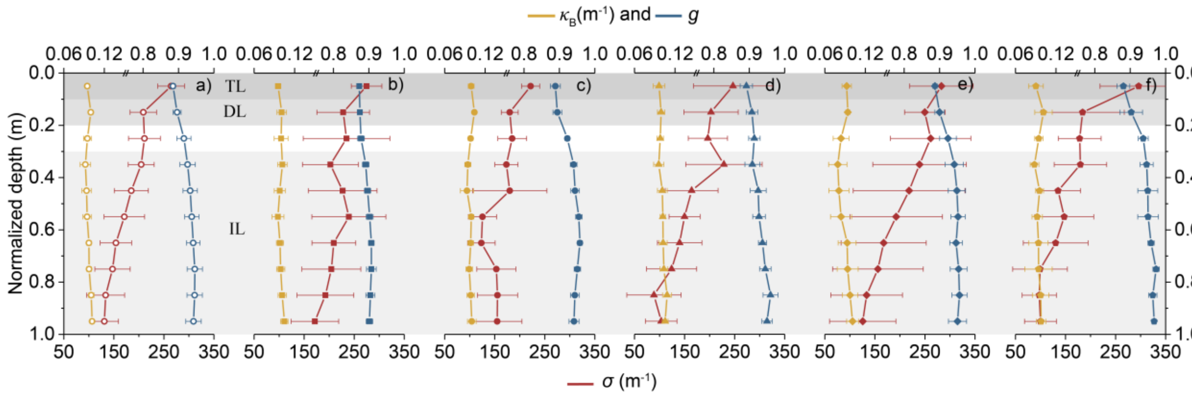

Figure 4. IOP profiles of ice cores against normalized depth in (a) the whole study period, (b) 2008, (c) 2010, (d) 2012, (e) 2014, and (f) 2016. The error bars show the standard deviation from the mean of the results.

The annual mean IOPs of the TL, DL, and IL of the ice cores are shown in Figure 5. As shown in Figure 5a, the variations in σ of the TL, DL, and IL were different. The variation in σ of the TL between years was statistically insignificant (ANOVA, $P > 0.1$), which reveals the relatively stable scattering ability of the ice surface. Things were different for IL, there are statistically significant variations in their σ between years (ANOVA, $P < 0.05$). Compared with 2008, the σ of the IL in 2016 decreased by 38.4% due to the decreased V_a (Figure 3). The overall variations in the σ of the DL were similar to that seen in the IL. Whereas, the former variations were not as clear as the latter one due to ongoing drainage, and were not significant (ANOVA, $P > 0.1$).

There were no statistically significant differences in the integrated absorption coefficient, κ_B, of the TL, DL, and IL (ANOVA, $P > 0.1$), indicating the absorptivity of ice in different depths is similar. Furthermore, the developments of κ_B in the three layers are similar (Figure 5b). Among the three layers, the statistical significance of changing κ_B of IL between years was relatively well (ANOVA, $P < 0.05$) than TL and DL. As shown in Figure 5c, the values of g of the TL and DL were nearly constant. Because their values of V_b were sufficiently small and similar due to drainage (Figure 3b), their values of g are mainly attributed to gas bubbles. In contrast, the g of IL varied significantly (ANOVA, $P < 0.01$). The values of g of the IL increased by 5% with increasing V_b in the study years (Figure 3b).

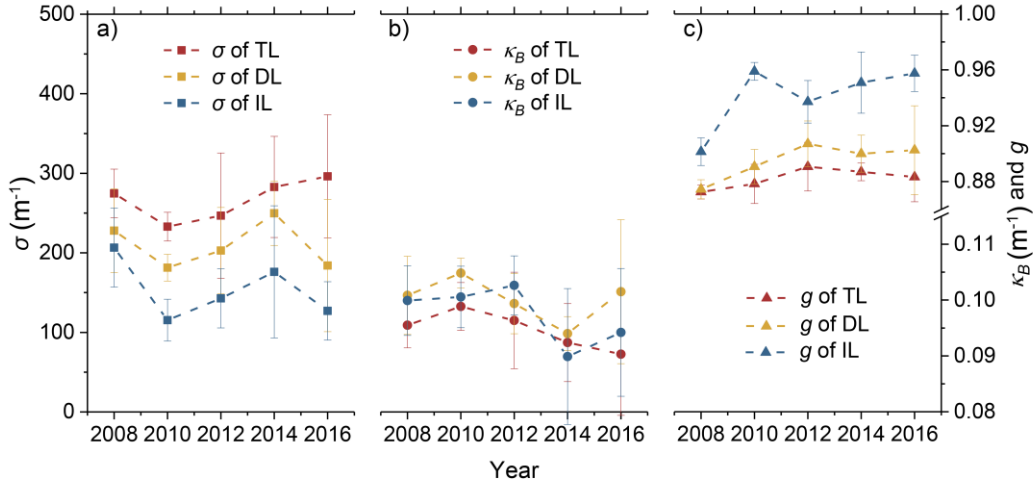

Figure 5. Annual (a) σ, (b) κ_B, and (c) g for the TL, DL, and IL of the ice cores from 2008 to 2016. The error bars show the standard deviation in each year.

3.3 Variations in the AOPs of the ice cores

Having seen that the IOP profiles of the sea ice were not constant in the different years (Figure 5), a more important question is how these changes affected the AOPs. The radiative transfer model was employed here to estimate the AOPs of sampling sites, as shown in Figure 6. Note that the AOPs here were calculated based on the level ice. Surface properties, such as a snow layer or melt ponds, were not considered here, because the focus was on the effects of the ice microstructure on their AOPs. The results obtained with the same IOPs profiles but for a constant ice thickness (1 m) are also presented to quantify the contributions from the ice microstructure and thickness separately.

It can be seen from Figure 6a that the thickness of ice cores decreased in study years with a statistically significant trend (r = -0.89, P < 0.05) and variations (ANOVA, P < 0.05). The values of α_B changed because of the effects of the ice IOPs and thickness (Figure 6b). The variations in mean α_B during 2008-2014 were similar to those in the σ of the TL and DL. In 2016, the mean α_B decreased due to the decreasing ice thickness. As a result, there are no statistically significant variations in α_B between years (ANOVA, P > 0.1). This was different from the remote-sensing results (-0.05 per decade for 1982 to 2009) of Lei et al. (2016). Part of the reason for this was the direct factor that reduces the annual ice albedo is not the ice microstructure but rather the surface conditions. Eicken et al. (2004) and Landy et al. (2015) reported that the evolution of melt ponds on the ice surface could explain 85% of the variance in the summer ice albedo.

Different from α_B, annual variations in T_B and A_B were significant (ANOVA, P < 0.05). The T_B (A_B) tended to increase (decrease) with years (Figure 6c). The mean value of T_B in 2016 was over treble of that in 2008. Meanwhile, A_B decreased by about 19.5% from 2008 to 2016. Furthermore, the change of A_B in the study years was lower than the actual change in the ice thickness (-35.0%). Thus the difference, 23.8% ($\frac{1-19.5\%}{1-35.0\%}-1$), was attributed to an increase in the absorbed solar energy per unit volume of sea ice. This result does match the findings of Light et al. (2015), which showed that the thickness of first-year ice was less by 13.3% than multiyear ice (1.3 m vs. 1.5 m, respectively). Whereas, the radiation absorbed by the former was less by 2% than the latter. In other words, the solar energy absorbed by a unit volume of first-year ice was greater than multiyear ice by 12.5%.

To make a direct comparison with the above variations, we considered a constant ice thickness, finding no clear changes in α_B (Figure 6b). Meanwhile, the variations in T_B and A_B were different clearly with similar overall trends (dashed lines in Figure 6c). T_B increased from 0.03 to 0.07 from 2008 to 2016, accounting for about 33.1% of the real change ratio with changing thickness. Thus, the changing microstructure of the melting ice resulted in an increased transmittance that was independent of the ice thickness. A similar result was observed in the laboratory, where the changing ice microstructure during the warming process (no decrease in thickness) increased the ice transmittance (Light et al., 2004). Different from T_B and A_B, whether the thickness was taken into account or not, the variations in α_B were hardly affected. This demonstrated that the present variations in ice thickness had more effects on the ice T_B and A_B than α_B.

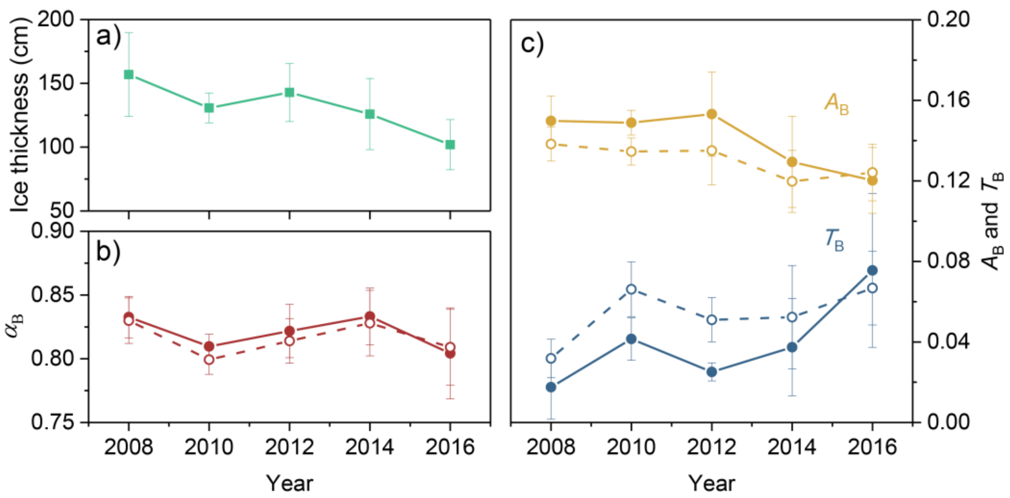

Figure 6. (a) Thickness and (b, c) estimated AOPs of the ice cores from 2008 to 2016. Also shown as dashed lines are the AOPs with the same IOPs and constant thickness (1 m). The error bars show the standard deviation in each year.

3.4 Arctic-wide analysis

In this section, to get the quantitative effects of varying IOPs on the radiation distribution of the Arctic with a real ice thickness field, we expand the variations of the ice cores (Figure 5) to an Arctic-wide scale under the following assumptions. First, the IOPs of Arctic ice were based on the results derived from the ice cores. This follows the common approach used in current models, i.e. they are taken as constant, and seasonal and spatial differences are ignored (e.g., Briegleb and Light, 2007).

Second, a decreasing trend of -5.8 cm yr^{-1} in ice thickness according to Lindsay and Schweiger (2015) was adopted to get a general view of the contributions of the changing ice thickness on the radiation budget. The representative basin-scale sea ice and radiation data in summer were used here to estimate the variations in the distribution of radiation fluxes.

With the combined effects of the changing microstructure and thickness of ice, Arctic-wide variations in the mean α_B, T_B, and A_B were statistically significant (ANOVA, $P < 0.01$) and clearer than those in Figure 6 (Figure 7a), especially the overall trends of the mean T_B ($r = 0.95$, $P < 0.01$) and A_B ($r = -0.98$, $P < 0.01$) of ice. Although the mean α_B decreased from 2008 to 2016, there was not much change in reflected solar flux (E_r), about 51.2 W m^{-2} during the study years (Figure 7b). This was resulted from that the decreasing α_B was largely provided by marginal ice zones. The decreasing rate of α_B in regions with ice thicknesses < 1 m (equivalent to 16.4% of the entire ice area) was over 1.6 times the rate of the entire ice cover (Figure S2). With the retreat of sea ice, the reflected flux of the marginal zone contributes less and less to the reflected flux of the entire ice cover.

Different from E_r, the overall trends of transmitted (E_t) and absorbed solar flux (E_a) were clear under the combined effects of the changing microstructure and ice thickness. The mean E_t, was significantly different between years (ANOVA, $P < 0.01$), and increased from 1.8 W m^{-2} to 9.0 W m^{-2} from 2008 to 2016 significantly ($r = 0.93$, $P < 0.05$, Figure 7b). Most of the increase in E_t is ascribed to thin ice in marginal ice zones (ice thicknesses < 1 m), which contributed 51.8% of the increasing E_t from 2008 to 2016 (Figure 8a–e). Meanwhile, variations in transmitted solar radiation E_a were significant (ANOVA, $P < 0.01$). The E_a decreased from 8.6 W m^{-2} in 2008 to 7.2 W m^{-2} in 2016 significantly ($r = -0.94$, $P < 0.05$). As the decrease in ice volume from 2008 to 2016 was 32.2%, the solar energy absorbed by a unit volume of sea ice increased by 23.4% on the Arctic scale.

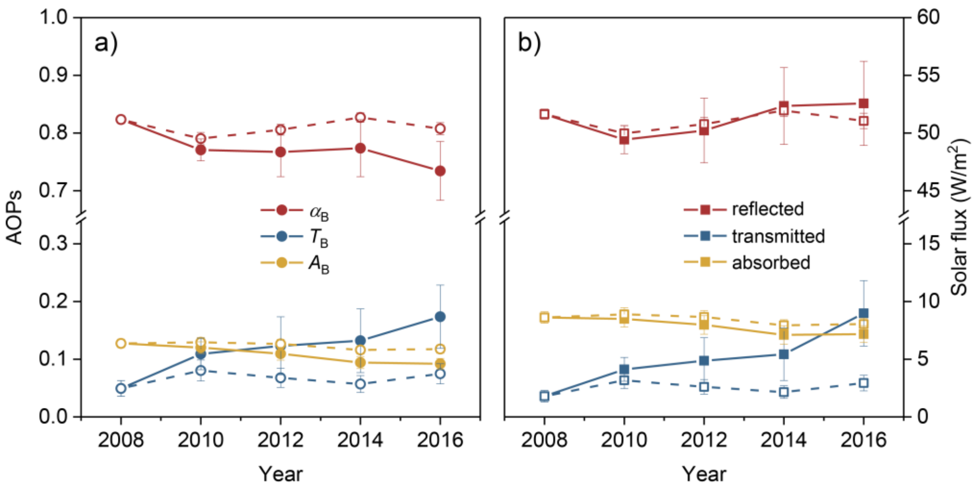

Figure 7. Arctic-wide variations in the mean (a) AOPs of ice and (b) solar flux distribution during 2008-2016. Also shown as dashed lines are the AOPs and fluxes with the same IOPs and constant thickness field. The error bars show the standard deviation in each year.

When the ice thickness was set as a constant, variations in the mean AOPs were different, which resulted in differences in the solar flux (dashed lines in Figure 7b). Among them, differences in the reflected flux E_r were relatively small. Meanwhile, the mean E_t increased from 1.8 W m^{-2} in 2008 to 2.9 W m^{-2} in 2016, with no significant trend. E_a decreased from 8.6 W m^{-2} to 8.0 W m^{-2} in the same period. These changes corresponded to 16.0% and 39.3% of the combined effects of the ice IOPs and thickness, respectively, from 2008 to 2016. Furthermore, marginal ice zones with ice thicknesses < 1 m still contributed 38.5% of the increasing E_t from 2008 to 2016 (Figure 8f-j). This value was about 74.3% of the rate of the combined effects of the changing IOPs and thickness of ice. In other words, the same changes in the ice microstructure had more effects on the T_B of thin sea ice, and these effects were clearer than those resulting from general decreasing ice thickness.

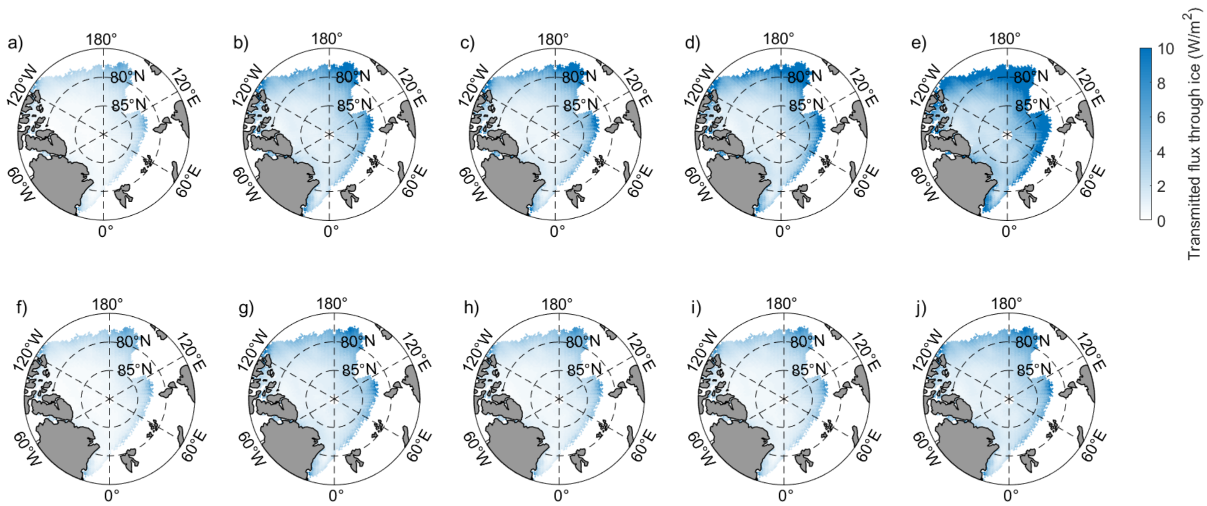

Figure 8. Distribution of transmitted solar radiation through sea ice in the summers of 2008 to 2016 when the sea ice thickness was set (a–e) to decrease and (f–j) to a constant value. Only flux that penetrated through the sea ice is considered in this map.

4 Discussion

4.1 Comparisons with IOP measurements

In Section 3.2, we estimated the ice IOPs according to the observed ice physics and structural-optical theory. Other methods estimated ice IOPs in previous studies. In this section, we compared the ice scattering coefficient, the most variable value among all IOPs, determined in the present study with previous results (Figure 9). The differences in wavelength bands were ignored in the comparisons because σ was nearly wavelength-independent.

It is clear from Figure 9 that the range of σ of the present study covered the majority of previous results. The derived values of σ for the SSL and DL of melting bare ice in August ranged from 920 to 2,000 m^{-1} and 40 to 150 m^{-1}, respectively (Light et al., 2008). According to the layer structure, wherein the TL was composed of a 5 cm SSL and the others were DLs, the bulk σ of the TL in Light et al. (2008) ranged from 270 to 435 m^{-1}. This result was slightly higher than our results. The results of Mobley et al. (1998) and Perron et al. (2021) agree with our range. The σ of the DL in Perron et al. (2021) was in our range, and the values of Light et al. (2008) were smaller than those in the present study.

Differences in the σ of the IL were clearer than in the TL and DL. The σ values of the IL of most our cores were relatively larger than those of Light et al. (2008, 2015) and Frantz et al (2019). In these results, Light et al. (2008) estimated the σ using the observed ice albedo and a three-layer structure with fixed thicknesses. The results of Light et al. (2015) and Frantz et al. (2019) were obtained in a cold laboratory by simulating the radiative transport in subsections of sea ice. Meanwhile, the results of Grenfell et al. (2006) and Perron et al. (2021) are close to the minimum of our range. The σ of ice in Grenfell et al., (2006) was calculated from the ice extinction coefficient, and it was measured *in situ* using a diffuse reflectance probe in the Perron et al. (2021). The values calculated by the same method as used in the present study by Mobley et al. (1998) were close to the maximum of our range. Thus, it was expected that the differences in the IL's σ partly resulted from the different methods used in the myriad studies.

One possible reason for the differences was the uncertainties in the ice microstructure introduced by brine loss during measurement and segmenting. Thus, our V_a values of the IL are greater than the values derived from nondestructive methods (e.g., Perron et al., 2021). As a result, the maximum underestimate of V_b was 15–25% and the maximum overestimate of V_a was 96–160% when taking the uncertainties introduced by the measurements and brine drainage into account (Wang et al., 2020). Taking the mean V_a and V_b of all ice cores as an example, these uncertainties overestimated the σ of the IL by 78 m^{-1} at most. Although brine loss during sampling and measurements introduced uncertainties to V_a and V_b, the methods used for obtaining and measuring the ice cores during the CHINARE cruises were the same. Therefore, the uncertainties introduced by the methodology hardly affected the changes seen in Figure 6 and Figure 7.

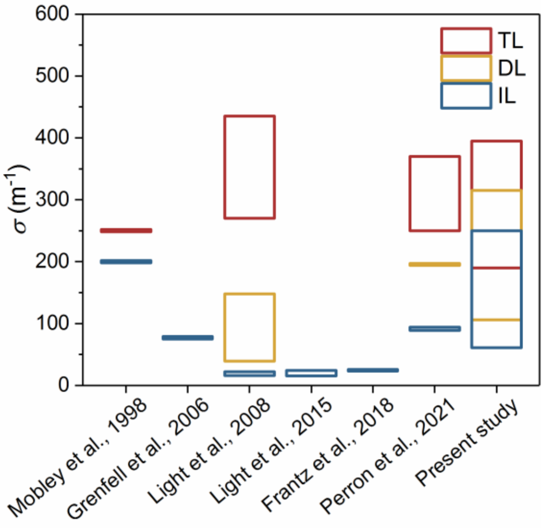

Figure 9. Comparison of the ice scattering coefficient in the present study to the published results for Arctic sea ice using various methods. All comparison results have been scaled to the layer structure used in the current study according to their ice thicknesses.

Another source of difference is the distribution function of gas bubbles employed in the IOP parameterization. Many distributions are obtained in a cold laboratory, where the ice temperature is not consistent with that in the summer Arctic. As the refractive indices of brines and pure ice were similar, the distribution function of brine pockets had a smaller influence on the ice IOPs than gas bubbles (Yu et al., 2022). Here, we tentatively adjusted the exponent of the distribution function of the gas bubbles from its default value of -1.5 to -1, i.e., the fraction of small bubbles decreases, which coincides with warming ice (Light et al., 2003). Then, the changed distribution function was used for 1 m thick ice with mean values of V_a and V_b for every ice core. This change resulted in an uncertainty of 8 m^{-1} in the σ of each layer. These uncertainties did not alter the above results and are considered acceptable.

Although brine loss and the difference in the distribution functions of gas bubbles introduced uncertainties in σ, they did not affect the ice AOPs much. Considering a 1 m thick ice layer described by the mean physics of ice cores, the effects of the former factor on the ice AOPs were less than 0.02. The uncertainties in α_B and T_B introduced by the latter factor were 0.005 and 0.002, respectively. Therefore, our estimated α_B range (0.76–0.87) agreed with the observed results of Light et al. (2008, 2015) and Grenfell et al. (2006). Meanwhile, the estimated T_B (0.01–0.1) was also in the corresponding observed ranges.

4.2 On the potential interannual variations of the IOPs

Extensive measurements of the IOPs of Arctic sea ice have been carried out, and some authors have noticed the seasonal variations of the ice microstructure and IOPs (e.g., Light et al., 2008; Frantz et al., 2019; Katlein et al., 2021). However, if there are interannual variations in sea ice IOPs are still not clear, although such changes in sea ice extent, thickness, and age are evident. A lack of continuous IOP measurements is the primary reason. Compared with previous observations, the ice core data in the present study were more appropriate for analyses on the potential interannual variations in ice IOPs because of their long time span and consistencies in the sampling method, seasons, and sea areas. The reason we could not introduce other ice core data (SHEBA, ICESCAPE, N-ICE, MOSAiC, etc.) into this study was that not only the differences in sampling seasons, sites, and methods increase the dispersion in time and space during such an analysis, but also the lack of information about the ice microstructure or essential physical properties will limit how much we can determine from such a comparison. We consider the presented ice core data is the best possible estimate on the potential interannual variations at this time, while acknowledging that further improvements of the data products are needed. Considering that sampling ice cores is a commonly used method for *in situ* observations, with more suitable ice core data in the future, large-scale time series of ice IOPs may be obtained.

The ice cores used in the present study were sampled at different ice stations but not at the same floe (Figure 1). That is, the data did not form a continuous observation in the strictest meaning. Thus, the variations shown in Section 3 can be regarded as the combined effects from three parts, i.e. spatial, temporal, and interannual variations. To do the discussion of interannual variability, it is necessary to first establish the spatial and temporal variability of ice cores. Figure 10 illustrates the different IOPs of the ice cores in three latitude zones, which shows that there are spatial differences in the present ice core data. Among the three IOPs, variations in σ are the clearest (up to 20%, Figure 10a). The differences in κ_B and g in the different latitude zones were not more than 5% and 3%, respectively (Figure 10b, c). As a transition layer between the TL and IL, variations in the IOPs of the DL were more discrete than in the other two layers. For now, we have little quantitative knowledge of the progressions of the sea ice IOPs and their influencing factors in the available literature. In the following discussion, the σ was set as the main content.

It can be seen from Figure 10a, there were no clear changes in the mean σ of TL in different latitude zones. Therefore, we ignore the spatial variations in σ of TL. We further discuss its whole variations in different years. The variability of the ice surface is directly related to the number of melt days. The melt days are affected by longwave radiation, water vapor, air temperature, and other factors (Persson, 2012; Mortin et al., 2016; Crawford et al., 2018). As shown in Figure 11a, the amount of surface downward longwave radiation during the study years was 300.2 ± 4.0 W/m^2 with no statistically significant trend (r = -0.57, P > 0.1), which is obtained from data reported by ECMWF. The total column vertically-integrated water vapor was also similar (11.9 ± 0.4 kg/m^2) with no significant trend (r = -0.58, P > 0.1). Different from the surface radiation, we found the observed air temperature increased at a speed of 0.14 ℃/year (r = 0.84, P < 0.1, Figure 11a). This clear difference in the temperatures was not an exception but a general circumstance in the Arctic during 2008–2016 (e.g., Collow et al., 2020). This could also be seen in the reanalysis data of ECMWF, where the mean air temperature in the summer of the study area has been increasing gradually (0.12 ℃/year, $r = 0.84$, $P < 0.1$). With the effects of several factors, the melting days of sampling sites, which were calculated according to the sampling date and melt onset from Markus et al. (2009), were 59 ± 7 days (Figure 11a). Their variation between years was statistically insignificant (ANOVA, $P > 0.1$). In other words, there are no significant differences in the surface melt of the ice cores in different years.

Previous observations demonstrated that ice surface melt was relatively weak in August (Perovich, 2003; Nicolaus et al., 2021). Macfarlane et al. (2023) further found that the SSL microstructure of melting ice has no temporal changes. Meanwhile, the difference in longwave radiation and vapor between sampling sites in single years were relatively small (Figure 11a). So, it is expected that the scattering coefficient of TL also has no clear seasonal variations. Whereas, an increasing scattering in the SSL during melt season was found in Light et al. (2008). This seems contrary to the finds of Macfarlane et al. (2023), but it is not. As stated in Light et al. (2008), the observed increase in scattering represents not only an increased scattering in a fixed depth layer but also an increased physical depth of the SSL or increased scattering of the next ice layer, because the modeled layer thickness was fixed. What was the same in the two studies was approximately constant albedo (or reflectance). This agrees with the similar albedo in Figure 6b of the present study, i.e. small seasonal differences don't affect the reflectivity of bare ice. For now, there was no theoretical explanation or quantitative description of the evolution of the microstructure of the ice surface during the melt (Petrich and Eicken, 2010). It can be seen from the present result, the increasing air temperature seems not the predominant affecting factor in the late melting season. In short, it is expected that the effects of temporal variations on the microstructure and IOPs of the ice surface were relatively small. Considering the whole variations in microstructure (Figure 3) and IOPs (Figure 5) were not significant, there are no clear temporal, spatial, or interannual variations in the ice surface of the present ice core data.

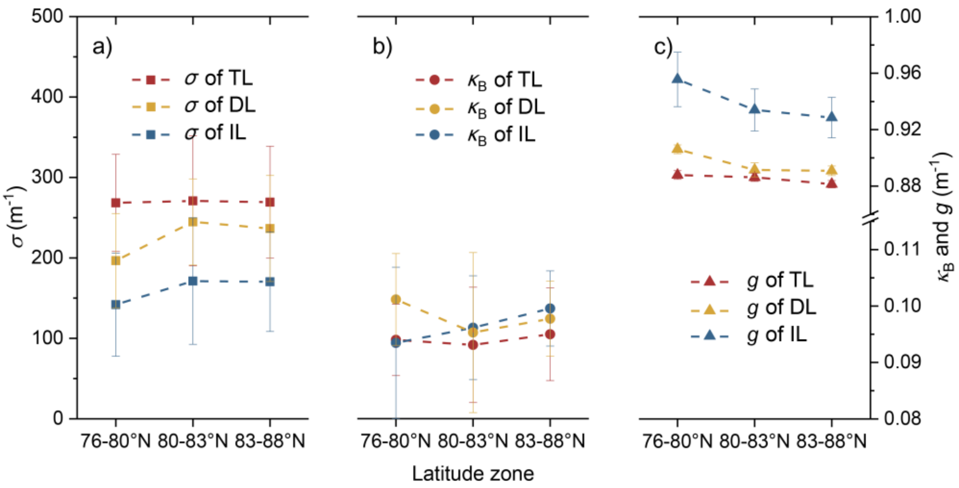

Figure 10. Different values of (a) σ, (b) κ_B, and (c) g for the TL, DL, and IL of the ice cores in the three latitude zones. The error bars show

the standard deviation in each latitude zone.

The σ of the IL is relatively constant during the entire melt season (Light et al., 2008). That's to say, the whole variations in the ice interior layer didn't result from temporal factors. Meanwhile, the latitudinal differences in the σ of the IL are clear. The σ of the ice IL in the low-latitude zone was relatively smaller than that in mid- or high-latitude zones (Figure 10a). This is expected that the ice at lower latitudes is generally warmer earlier, which increases the brine inclusion size and connectivity of ice. Then naturally reduced the ice scattering coefficient. The spatial variation of mean σ in the IL can be up to 30 m^{-1} between low-latitude and mid- or high-latitude zone. This value was equivalent to 32.9% of the maximum of the whole variation. This implied that the spatial and interannual variations in ice properties together result in the changing IOPs shown in Figure 5. So, it is necessary to exclude the spatial variations before discussing the interannual changes of σ. According to the propagation law of variation, the square of whole variations of IL-σ can be expressed as the square sum of their spatial variations and interannual variations. For the convenience of calculation, we ignored the small difference IL-σ between mid- and high-latitude zones. There are five and three cores in 2014 and 2016 sampled in the low-latitude zone, respectively. According to the differences between ice cores from different years (whole variations, Figure 3) and different latitude zones (spatial variations, Figure 10a), we correct the mean σ of the IL in 2014 from 176 m^{-1} to 182 m^{-1}. That's to say, the interannual variations were larger than the whole variations by 6 m^{-1}. The value of 2016 was also corrected from 127 m^{-1} to 131 m^{-1} accordingly. Then, variations among the corrected σ of the IL could be regarded as the result of the interannual factors.

Then, the corrected σ of the IL was used to discuss the interannual changes. Figure 11b shows the correlations among the corrected σ of the IL, ice age, and T_B in study years. Also shown in circles were the uncorrected σ of IL in 2014 and 2016. Note that T_B here is the result under the assumption of a constant ice thickness (dashed line in Figure 6c). The ice ages were obtained according to fieldwork (Wang et al., 2020) and remote-sensing data (Tschudi et al., 2019). Because the ice age of each grid cell in the remote-sensing data is represented as the age of the oldest floe, once an ice core was distinguished as first-year ice in the fieldwork, the corresponding ice age was set as one year regardless of the remote-sensing data. The use of remote-sensing data is acceptable because the ice cores in this study were all sampled in large and thick floes for safe fieldwork. These floes were more likely older than the surrounding ice. Figure 11b demonstrates that the decrease in the σ of the IL is significantly correlated with changing ice age ($r = 0.95$, $P < 0.01$). In other words, the ice age largely manifested in the ice microstructure in the IL. A similar result was also observed i.e. the σ of the IL in the first-year ice was smaller than in multiyear ice (e.g. Light et al. 2015). This could also partly explain the spatial variations in the σ of the IL (Figure 10a) because sea ice in high-latitude zones was likely older than in the other zones (Stroeve and Notz, 2018). Furthermore, there are significant correlations between σ of the IL and ice T_B (r = -0.93, P < 0.05). That's to say, the changing ice age can be responsible for the modeled results of changing ice transmittance shown in Figure 7, even without any decrease in the ice thickness. And one other thing to point out, the changing ice age seems to not affect the albedo of bare ice (Figure 6b). Light et al. (2022) suggest that the principal reason for this is the SSL shows invariance across location, decade, and ice age, which was confirmed by comparing data from MOSAiC (2019-2020) and SHEBA (1997-1998). Our results partly prove this view i.e. there are significant variations in the ice age but no significant variations in microstructure or IOPs of TL during 2008-2016.

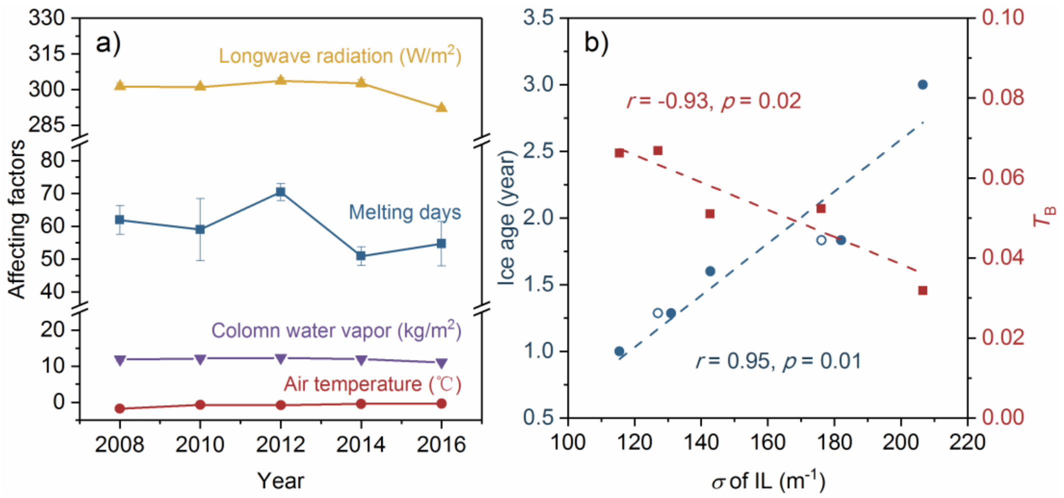

Figure 11. (a) Changing melting days, surface downward longwave radiation flux, total column vertically-integrated water vapor, and observed air temperature at the sampling sites. The error bars show the standard deviation in each year. Some error bars are invisible because they are small enough. (b) Correlations among the σ of the IL with ice age and T_B. The circles denote the uncorrected data.

In summary, we didn't find significant variations in the IOPs of the ice top layer. Meanwhile, the differences in the IOPs of the ice IL were related to interannual variations in the ice age. To our knowledge, this is the first study to link ice microstructure and optical properties at interannual scales. Although these ice core data are not a time series in the strictest meaning, they are still helpful for understanding the general effects of the scenario where the Arctic ice ages are decreasing. Our results suggested that in this scenario, the σ values of the IL of summer ice tended to be smaller than before. It is expected to lead to interannual trends of the ice microstructure and IOPs. Then, more solar radiation transmits into the ocean. The effects of this process need more attention in future observations and simulations.

4.3 Implications for the future Arctic

Previous studies have reported that surface properties (snow, ponds, etc.) largely control the variations in the ice albedo (Landy et al., 2015). The present results also asserted that variations in the ice's microstructure or IOPs had little effect on the albedo of bare ice (< 2%), but they do play an important role in ice transmittance (Figure 6). With continued Arctic warming, the summer ice age is on the decrease, and the ice microstructure and IOPs change accordingly, leading to an overall higher ice transmittance. Furthermore, the transmitted solar energy affects the temperature of the upper ocean and results in further melting of the bottom of sea ice (Timmermans, 2015). Along with the melting of ice, gas bubbles, and brine pockets change simultaneously (Light et al., 2004), which affects the IOPs of ice in turn. Consequently, the sea ice is expected to become thinner and more porous than before. This process has been seldom considered in previous studies. Related studies generally regarded the surface properties and thickness of the ice as predictors for light transmittance (e.g., Katlein et al., 2015; Perovich et al., 2020). The microstructure and morphological parameters of sea ice (e.g., thickness, extent, etc.) may together influence the melting processes of Arctic sea ice.

For safe field observations, the ice core data used in this study were all sampled in large and thick floes. Therefore, variations in the microstructure of the ice in marginal zones or under melt ponds cannot be addressed by this study. Light et al. (2015) reported that the differences in the σ between the IL of ponded first-year ice and multiyear ice were larger than those between bare first-year ice and multiyear ice. Therefore, the changes in the IOPs of the marginal ice zone were expected to be more obvious than those found in the present results because the ice in marginal zones is more likely young and ponded (Rigor and Wallace, 2004; Zhang et al., 2018). Furthermore, the same changes in the ice microstructure have more effects on the T_B of thin sea ice (Section 3.4). Marginal ice zones, comprising 16.4% of the entire ice area, contributed 39.3% of the extra-transmitted solar energy due to the ice changing microstructure from 2008 to 2016 (Figure 8). Both processes promote an increase of transmitted flux through sea ice and ice bottom melting in marginal ice zones. Arndt & Nicolaus (2014) quantified light transmittance through the sea ice into the ocean for all seasons as a function of variable sea ice types. The mean annual trend was 1.5% per year, which mainly depended on the timing of melt onset. If the variations in the microstructure of bare and ponded ice are taken into consideration, this trend is expected to increase. We suggest that future ice observations and models should pay more attention to variations in the ice age, microstructure, and their effects, especially in marginal ice zones.

5 Conclusions

This is the first study to link the ice microstructure, IOPs, and AOPs at interannual scales. Based on ice cores sampled during the CHINARE expeditions (2008–2016), the variations in the IOPs of Arctic sea ice in summer due to the changing microstructure of ice were modeled according to structural-optical theory. Variations in the AOPs and solar flux distribution due to the changing IOPs in the summer Arctic were also estimated. Clear variations in the microstructure and IOPs of each year (Figure 5) enabled us to construct a quantitative view of changes that the Arctic sea ice interior underwent in these years.

As a result of our study, there were no significant variations in the microstructure and IOPs of ice TL. This is related to the stable melt days in study years. Because σ of the upper layers (TL and DL) mainly control the albedo of bare ice, the variations in α_B between years were relatively small. Meanwhile, variations in the microstructure and IOPs of IL were significant. These variations consist mainly of interannual factors and minor spatial factors. After excluding the effects of spatial variations, we found these interannual variations in σ of ice IL were highly related to the changing ice ages. That's to say, the ice age largely manifested in the ice microstructure of the IL. The changing σ of ice IL affects the ice transmittance clearly. Furthermore, the same changes in the ice IOPs had more effects on the transmittance of the thin ice in marginal ice zones.

Previous studies paid more attention to changing transmittance due to declining ice thickness. The present findings demonstrated that the changing IOPs of interior ice derived from the ice microstructure could also alter the partitioning of solar radiation in sea ice by itself. With continued Arctic warming, summer ice will become younger and more porous than before, leading to more light reaching the upper ocean. This reminds us to pay more attention to the variations in the IOPs of interior ice, especially ice with different ages.

Acknowledgments. We are grateful to the NSIDC, Alfred Wegener Institute, and ECMWF for providing the sea ice and radiation data. This work was financially supported by the National Key Research and Development Program of China (Grant number 2018YFA0605901), the National Natural Science Foundation of China (Grant numbers 41922045, 41906198, 41976219, and 41876213), and the Academy of Finland (Grant numbers 333889, 325363, and 317999). We also wish to acknowledge the crews of the R/V Xuelong for their fieldwork during CHINARE.

Author contributions. MY carried out the estimations and wrote the paper. RL, BL, and QW provided the ice core data. All coauthors discussed the results and edited the manuscript.

Data Availability Statement. The sea ice and radiation data are available at https://doi.org/10.5067/MPYG15WAA4WX; https://data.meereisportal.de/gallery/index_new.php?lang=en_US&ice-type=extent&active-tab1=measurement&active-tab2=thickness; https://cds.climate.copernicus.eu/cdsapp#!/dataset/reanalysis-era5-single-levels-monthly-means?tab=form.The ice cores data applied in this work can be accessed in Wang et al. (2020).

Competing interests. The authors declare that they have no conflict of interest

References:

Arndt, S. and Nicolaus, M., 2014. Seasonal cycle and long-term trend of solar energy fluxes through Arctic sea ice. The Cryosphere, 8 (6): 2219-2233. doi:10.5194/tc-8-2219-2014

Briegleb, B. P. and Light, B., 2007. A Delta-Eddington Multiple Scattering Parameterization for Solar Radiation in the Sea Ice Component of the Community Climate System Model (No. NCAR/TN-472+STR). University Corporation for Atmospheric Research. doi:10.5065/D6B27S71

Carnat, G. and Papakyriakou, T., et al., 2013. Investigations on physical and textural properties of Arctic first-year sea ice in the Amundsen Gulf, Canada, November 2007 – June 2008 (IPY-CFL system study). Journal of Glaciology, 59 (217): 819-837. doi:10.3189/2013JoG12J148

Cole, D. M. and Eicken, H., et al., 2004. Observations of banding in first-year Arctic sea ice. Journal of Geophysical Research: Oceans, 109 (C8): n/a-n/a. doi:10.1029/2003JC001993

Collow, A. B. and Cullather, R. I., et al., 2020. Recent Arctic Ocean Surface Air Temperatures in Atmospheric Reanalyses and Numerical Simulations. Journal of Climate, 33 (10): 4347-4367. doi:10.1175/JCLI-D-19-0703.1

Comiso, J. C. and Parkinson, C. L., et al., 2008. Accelerated decline in the Arctic sea ice cover. Geophysical Research Letters, 35 (1): L01703. doi:10.1029/2007GL031972

Crabeck, O. and Galley, R. J., et al., 2019. Evidence of Freezing Pressure in Sea Ice Discrete Brine Inclusions and Its Impact on Aqueous - Gaseous Equilibrium. Journal of Geophysical Research: Oceans, 124 (3): 1660-1678. doi:10.1029/2018JC014597

Crabeck, O. and Galley, R., et al., 2016. Imaging air volume fraction in sea ice using non-destructive X-ray tomography. The Cryosphere, 10 (3): 1125-1145. doi:10.5194/tc-10-1125-2016

Crawford, A. D. and Horvath, S., et al., 2018. Modulation of Sea Ice Melt Onset and Retreat in the Laptev Sea by the Timing of Snow Retreat in the West Siberian Plain. Journal of Geophysical Research: Atmospheres, 123 (16): 8691-8707. doi:10.1029/2018JD028697

Dai, A. and Luo, D., et al., 2019. Arctic amplification is caused by sea-ice loss under increasing CO2. Nature Communications, 10 (1). doi:10.1038/s41467-018-07954-9

DiGirolamo, N. E. and Parkinson, C., et al., 2022. updated yearly. Sea Ice Concentrations from Nimbus-7 SMMR and DMSP SSM/I-SSMIS Passive Microwave Data, Version 2. Boulder, Colorado USA. NASA National Snow and Ice Data Center Distributed Active Archive Center..

Ehn, J. K. and Papakyriakou, T. N., et al., 2008. Inference of optical properties from radiation profiles within melting landfast sea ice. Journal of Geophysical Research, 113: C09024. doi:10.1029/2007JC004656

Eicken, H. and Grenfell, T. C., et al., 2004. Hydraulic controls of summer Arctic pack ice albedo. Journal of Geophysical Research: Oceans, 109 (C08007): n/a-n/a. doi:10.1029/2003JC001989

Eicken, H. and Lensu, M., et al., 1995. Thickness, structure, and properties of level summer multiyear ice in the Eurasian sector of the Arctic Ocean. Journal of Geophysical Research, 100 (C11): 22697-22710. doi:10.1029/95JC02188

Frantz, C. M. and Light, B., et al., 2019. Physical and optical characteristics of heavily melted "rotten" Arctic sea ice. The Cryosphere, 13 (3): 775-793. doi:10.5194/tc-2018-141

Frantz, C. M. and Light, B., et al., 2019. Physical and optical characteristics of heavily melted “rotten” Arctic sea ice. The Cryosphere, 13 (3): 775-793. doi:10.5194/tc-13-775-2019

Grenfell, T. C., 1983. A theoretical model of the optical properties of sea ice in the visible and near infrared. Journal of Geophysical Research: Oceans, 88 (C14): 9723-9735. doi:10.1029/JC088iC14p09723

Grenfell, T. C., 1991. A radiative transfer model for sea ice with vertical structure variations. Journal of Geophysical Research: Oceans, 96 (C9): 16991-17001. doi:10.1029/91JC01595

Grenfell, T. C. and Light, B., et al., 2006. Spectral transmission and implications for the partitioning of shortwave radiation in arctic sea ice. Annals of glaciology, 44 (1): 1-6. doi:10.3189/172756406781811763

Grenfell, T. C. and Perovich, D. K., 1981. Radiation Absorption Coefficients of Polycrystalline ice from 400 to 1400 nm. Journal of Geophysical Research, 86 (C8): 7447-7450. doi:10.1029/2007JD009744

Grenfell, T. C. and Perovich, D. K., 2008. Incident spectral irradiance in the Arctic Basin during the summer and fall. Journal of Geophysical Research, 113: D12117. doi:10.1029/2007JD009418

Grenfell, T. C. and Warren, S. G., 1999. Representation of a nonspherical ice particle by a collection of independent spheres for scattering and absorption of radiation. Journal of Geophysical Research, 104 (D24): 31697-31709. doi:10.1029/1999JD900496

Hamre, B., 2004. Modeled and measured optical transmittance of snow-covered first-year sea ice in Kongsfjorden, Svalbard. Journal of Geophysical Research, 109 (C10). doi:10.1029/2003JC001926

Hansen, J. E. and Travis, L. D., 1974. Light scattering in planetary atmosphere. Space Science Reviews, 16: 527-610. doi:10.1007/BF00168069

Hunke, E. C. and Notz, D., et al., 2011. The multiphase physics of sea ice: a review for model developers. The Cryosphere, 5 (4): 989-1009. doi:10.5194/tc-5-989-2011

Katlein, C. and Arndt, S., et al., 2015. Influence of ice thickness and surface properties on light transmission through Arctic sea ice. Journal of Geophysical Research: Oceans, 120 (9): 5932-5944. doi:10.1002/2015JC010914

Katlein, C. and Arndt, S., et al., 2019. Seasonal Evolution of Light Transmission Distributions Through Arctic Sea Ice. Journal of Geophysical Research: Oceans, 124 (8): 5418-5435. doi:10.1029/2018JC014833

Katlein, C. and Valcic, L., et al., 2021. New insights into radiative transfer within sea ice derived from autonomous optical propagation measurements. The Cryosphere, 15 (1): 183-198. doi:10.5194/tc-15-183-2021

Kwok, R., 2018. Arctic sea ice thickness, volume, and multiyear ice coverage: losses and coupled variability (1958-2018). Environmental research letters, 13 (10): 105005. doi:10.1088/1748-9326/aae3ec

Kwok, R. and Cunningham, G. F., 2016. Contributions of growth and deformation to monthly variability in sea ice thickness north of the coasts of Greenland and the Canadian Arctic Archipelago. Geophysical Research Letters, 43 (15): 8097-8105. doi:10.1002/2016GL069333

Landy, J. C. and Ehn, J. K., et al., 2015. Albedo feedback enhanced by smoother Arctic sea ice. Geophysical Research Letters, 42 (24): 10,714-10,720. doi:10.1002/2015GL066712

Lei, R. and Tian-Kunze, X., et al., 2016. Changes in summer sea ice, albedo, and portioning of surface solar radiation in the Pacific sector of Arctic Ocean during 1982-2009. Journal of Geophysical Research: Oceans, 121 (8): 5470-5486. doi:10.1002/2016JC011831

Light, B. and Grenfell, T. C., et al., 2008. Transmission and absorption of solar radiation by Arctic sea ice during the melt season. Journal of Geophysical Research, 113: C03023. doi:10.1029/2006JC003977

Light, B. and Maykut, G. A., et al., 2003. Effects of temperature on the microstructure of first-year Arctic sea ice. Journal of Geophysical Research: Oceans, 108 (C2): 3051. doi:10.1029/2001JC000887

Light, B. and Maykut, G. A., et al., 2004. A temperature-dependent, structural-optical model of first-year sea ice. Journal of Geophysical Research, 109: C06013. doi:10.1029/2003JC002164

Light, B. and Perovich, D. K., et al., 2015. Optical properties of melting first‐year Arctic sea ice. Journal of Geophysical Research: Oceans, 120 (11): 7657-7675. doi:10.1002/2015JC011163

Light, B. and Smith, M. M., et al., 2022. Arctic sea ice albedo: Spectral composition, spatial heterogeneity, and temporal evolution observed during the MOSAiC drift. Elementa: Science of the Anthropocene, 10 (1). doi:10.1525/elementa.2021.000103

Lindsay, R. and Schweiger, A., 2015. Arctic sea ice thickness loss determined using subsurface, aircraft, and satellite observations. The Cryosphere, 9 (1): 269-283. doi:10.5194/tc-9-269-2015

Macfarlane, A. R. and Dadic, R., et al., 2023. Evolution of the microstructure and reflectance of the surface scattering layer on melting, level Arctic sea ice. Elementa: Science of the Anthropocene, 11 (1). doi:10.1525/elementa.2022.00103

Markus, T. and Stroeve, J. C., et al., 2009. Recent changes in Arctic sea ice melt onset, freezeup, and melt season length. Journal of Geophysical Research, 114: C12024. doi:10.1029/2009JC005436

Mobley, C. D. and Cota, G. F., et al., 1998. Modeling Light Propagation in Sea Ice. IEEE Transactions on Geoscience and Remote Sensing, 36 (5): 1743-1749. doi:10.1109/36.718642

Mortin, J. and Svensson, G., et al., 2016. Melt onset over Arctic sea ice controlled by atmospheric moisture transport. Geophysical Research Letters, 43 (12): 6636-6642. doi:10.1002/2016GL069330

Nicolaus, M. and Hoppmann, M., et al., 2021. Snow depth and air temperature seasonality on sea ice derived from snow buoy measurements. Frontiers in Marine Science, 8. doi:10.3389/fmars.2021.655446

Notz, D. and Worster, M. G., 2009. Desalination processes of sea ice revisited. Journal of Geophysical Research, 114 (C5). doi:10.1029/2008JC004885

Parkinson, C. L. and Comiso, J. C., 2013. On the 2012 record low Arctic sea ice cover: Combined impact of preconditioning and an August storm. Geophysical Research Letters, 40 (7): 1356-1361. doi:10.1002/grl.50349

Perovich, D. K., 2003. Complex yet translucent: the optical properties of sea ice. Physica B: Condensed Matter, 338 (1-4): 107-114. doi:10.1016/S0921-4526(03)00470-8

Perovich, D. K., 2003. Thin and thinner: Sea ice mass balance measurements during SHEBA. Journal of Geophysical Research, 108 (C3). doi:10.1029/2001JC001079

Perovich, D. and Light, B., et al., 2020. Changing ice and changing light: trends in solar heat input to the upper Arctic ocean from 1988 to 2014. Annals of Glaciology, 61 (83): 401-407. doi:10.1017/aog.2020.62

Perron, C. and Katlein, C., et al., 2021. Development of a diffuse reflectance probe for in situ measurement of inherent optical properties in sea ice. The Cryosphere, 15 (9): 4483-4500. doi:10.5194/tc-15-4483-2021

Persson, P. O. G., 2012. Onset and end of the summer melt season over sea ice: thermal structure and surface energy perspective from SHEBA. Climate Dynamics, 39 (6): 1349-1371. doi:10.1007/s00382-011-1196-9

Petrich, C. and Eicken, H., 2010. Growth, Structure and Properties of Sea Ice in Thomas, DN, Dieckmann, GS eds., Sea ice. 2nd ed. Hoboken, NJ: Wiley Online Library.

Petty, A. A. and Stroeve, J. C., et al., 2018. The Arctic sea ice cover of 2016: a year of record-low highs and higher-than-expected lows. The Cryosphere, 12 (2): 433-452. doi:10.5194/tc-12-433-2018

Ricker, R. and Hendricks, S., et al., 2017. A weekly Arctic sea-ice thickness data record from merged CryoSat-2 and SMOS satellite data. The Cryosphere, 11 (4): 1607-1623. doi:10.5194/tc-11-1607-2017

Rigor, I. G. and Wallace, J. M., 2004. Variations in the age of Arctic sea-ice and summer sea-ice extent. Geophysical Research Letters, 31 (9): n/a-n/a. doi:10.1029/2004GL019492

Smedley, A. R. D. and Evatt, G. W., et al., 2020. Solar radiative transfer in Antarctic blue ice: spectral considerations, subsurface enhancement, inclusions, and meteorites. The Cryosphere, 14 (3): 789-809. doi:10.5194/tc-14-789-2020

Smith, M. M. and Light, B., et al., 2022. Sensitivity of the Arctic Sea Ice Cover to the Summer Surface Scattering Layer. Geophysical Research Letters, 49 (9): e2022GL098349. doi:10.1029/2022GL098349

Smith, R. C. and Baker, K. S., 1981. Optical properties of the clearest natural waters (200 – 800 nm). Applied Optics, 20 (2): 177. doi:10.1364/AO.20.000177

Stroeve, J. and Notz, D., 2018. Changing state of Arctic sea ice across all seasons. Environmental research letters, 13 (10): 103001. doi:10.1088/1748-9326/aade56

Timmermans, M. L., 2015. The impact of stored solar heat on Arctic sea ice growth. Geophysical Research Letters, 42 (15): 6399-6406. doi:10.1002/2015GL064541

Tschudi, M. A. and Meier, W. N., et al., 2020. An enhancement to sea ice motion and age products at the National Snow and Ice Data Center (NSIDC). The Cryosphere, 14 (5): 1519-1536. doi:10.5194/tc-14-1519-2020

Tschudi, M. and Meier, W., et al., 2019. EASE-Grid Sea Ice Age, Version 4. [Indicate subset used]. Boulder, Colorado USA. NASA National Snow and Ice Data Center Distributed Active Archive Center.. doi:10.5067/UTAV7490FEPB

Tucker, W. B. and Perovich, D. K., et al.,1992. Physical Properties of Sea Ice Relevant to Remote Sensing. Microwave Remote Sensing of Sea Ice, American Geophysical Union: 9-28.

Vancoppenolle, M. and Fichefet, T., et al., 2009. Simulating the mass balance and salinity of Arctic and Antarctic sea ice. 2. Importance of sea ice salinity variations. Ocean Modelling, 27 (1-2): 54-69. doi:10.1016/j.ocemod.2008.11.003

Veyssière, G. and Castellani, G., et al., 2022. Under-Ice Light Field in the Western Arctic Ocean During Late Summer. Frontiers in Earth Science, 9. doi:10.3389/feart.2021.643737

Wang, Q. and Lu, P., et al., 2020. Physical Properties of Summer Sea Ice in the Pacific Sector of the Arctic During 2008 – 2018. Journal of Geophysical Research: Oceans, 125 (9). doi:10.1029/2020JC016371

Weeks, W. F. and Ackley, S. F., 1986. The Growth, Structure, and Properties of Sea Ice.

Yu, M. and Lu, P., et al., 2022. Impact of Microstructure on Solar Radiation Transfer Within Sea Ice During Summer in the Arctic: A Model Sensitivity Study. Frontiers in marine science, 9 (861994). doi:10.3389/fmars.2022.861994

Zhang, J. and Schweiger, A., et al., 2018. Melt Pond Conditions on Declining Arctic Sea Ice Over 1979 – 2016: Model Development, Validation, and Results. Journal of Geophysical Research: Oceans, 123 (11): 7983-8003. doi:10.1029/2018JC014298